Spin Hall Angles in Solids Exhibiting a Giant Spin Hall Effect

BROWN

Jamie Holber
Thesis Advisor: Professor Gang Xiao
Department of Physics
Brown University

A thesis submitted in fulfillment
for the degree of Bachelor of Science in Physics
April 2019

Abstract

The Spin Hall Effect enables the conversion of charge current into spin current and provides a method for electrical control of the magnetization of a ferromagnet, enabling future applications in the transmission, storage, and control of information. The experimental values found for the Spin Hall Angle (Θ_{SH}), a way of quantifying the Spin Hall Effect in a nonmagnetic material, are studied in this thesis in regards to a variety of parameters including the atomic number, the fullness of the orbital, the spin diffusion length, thin film thickness, resistivity, temperature, and composition of alloys. We observed that the spin Hall angle dependence on atomic number, the fullness of the orbital, the spin diffusion length, and the resistivity aligned with the theory. The dependence on thickness and temperature was found to vary based on the material and more research is needed to determine larger trends. We found that alloys provide opportunities to create materials with large spin hall angles with lower resistivities. In particular, Au alloyed with other elements is a promising candidate.

Acknowledgements

Thanks to my advisor, Professor Gang Xiao for his time and guidance working on my thesis. I would also like to thank the other members of my lab group who helped me and helped work on the project, Lijuan Qian, Wenzhe Chen, Guanyang He, Yiou Zhang, and Kang Wang. And finally, thanks to my family and friends who helped me along the way.

Contents

List of Figures

Chapter 1:
Introduction and Background

Information is most commonly stored as binary numbers, where a bit represents either a 0 or 1. In electronics, the state of a transistor is used to represent one bit. Charges are moved by electric fields to transmit the data and change the state of the transistor [2]. Conventional electronics rely only on the electron charge and can be volatile, leading to high power consumption.

Spin electronics or spintronics is the study of the intrinsic spin of an electron and its associated magnetic moment. The field of spintronics utilizes both the spin and the charge degrees of freedom of an electron with the goal of manipulating, creating, and detecting spin currents to be used in the field of magnetic electronics and for information technologies[3, 4]. Spintronics has many advantages over electronics, including non-volatility, low power dissipation, fast speeds, and large storage density; leading to the possibility of the continuation of Moore's Law[5].

Spintronics has already impacted the field of information technology with the development of high density magnetic recording, non-volatile solid state memory, magnetoresitive sensors, and spin values used in magnetic hard disk drives[4, 6, 7]. Furthermore, spintronics is expected to contribute to the efficiency and development of many technologies including magnetic random access memories (MRAM), spin logics (SL), rf devices, magneto-optical components, universal memory, and magnetic tunnel junctions(MTJs)[1, 4, 8].

The development of spintronics as a major field of research in the 1980s was prompted by the discovery of the giant magnetoresistance effect, allowing for efficient spin-dependent transport[6]. Over time, spintronics has evolved from the study of spin polarized currents to pure spin currents. Pure spin currents have no stray Oersted fields, leading to minimal power dissipation, and therefore low power consumption and high efficiency[5, 9, 10]. In order to easily integrate spin currents with existing technology it is necessary that the spin current be controllable and readable using charge signals [5]. The Spin Hall Effect (SHE) is one possible mechanism for the creation and control of spin currents. Although, for most metals the conversion efficiency of the SHE is a few percent, several materials exhibit a Giant Spin Hall Effect (GSHE), where a conversion efficiency has been seen as large as 60%, making them optimal candidates for the efficient generation and control of spin currents.

The SHE converts a charge current passing through a non-magnetic (NM) material into a transverse pure spin current. This effect arises from spin-dependent deflection due to spin-orbit coupling resulting in the lateral surfaces of the NM being oppositely polarized[3, 9], as seen in Figure 1.1. The SHE is often utilized in Ferromagnet (FM)-NM bilayers by generating a pure spin current in the NM layer, which then exerts a spin-transfer torque(STT) on the FM layer. Above a critical current density the FM switches orientation quickly via domain wall polarization [8, 1]. Therefore, utilizing

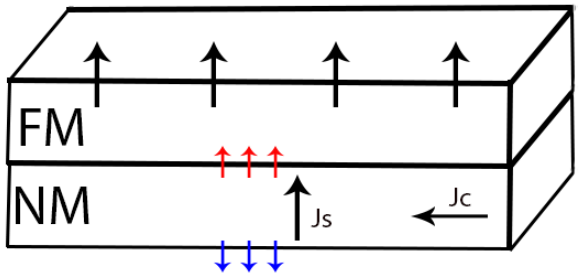

Figure 1.1: Diagram of the Spin Hall Effect in a NM-FM bilayer. The electrons from the charge current(J_c) experience spin-dependent deflection leading to the lateral edges of the NM having opposite polarization creating a spin current(J_s).

the SHE we should be able to control the magnetization of the FM with only a small electrical current.

Many spintronic applications rely on FM because the electron spins behave collectively and will keep their polarization, making them easier to manipulate [7]. This is the application that will be focused on in this thesis.

1.1 Spin-Orbit Coupling

One of the most important principles for the SHE is spin-orbit interaction or spin-orbit coupling (SOC). The theory for this section is largely taken from reference [11]. SOC is the interaction of a particle's spin with its motion inside an atomic potential or the potential of a nucleus. This creates an effective magnetic field leading to a shift in the electron's energy level and the electron's orbital angular momentum. The Hamiltonian of a spin-orbit coupling interaction is:

$$H_{SO} = -\boldsymbol{\mu_s} \cdot \mathbf{B_{SO}} \tag{1.1}$$

where μ_s is the magnetic moment of the electron, and B_{SO} is the magnetic field due to the potential. The magnetic field can arise from several mechanisms as discussed below.

1.1.1 Spin Orbit Coupling during scattering

In a vacuum an electron, with magnetic moment μ_s, will experience a magnetic field (B_{SO}) due to the angular movement of the nucleus in the electron's reference frame. The magnetic field is proportional to the momentum of the electron as described by the Biot-Savart Law.

The spin-orbit Hamiltonian arises from the Zeeman interaction of μ_s and B_{SO} and is dependent on the angular momentum of the electron($\mathbf{L}$) the electron spin state ($\mathbf{S}$), the number of protons in the nucleus (Z), and the radius(r):

$$H_{SO} = \frac{g_0 \mu_B^2 Z}{r^3 \hbar^2} \mathbf{S} \cdot \mathbf{L} \tag{1.2}$$

where g_0 is the electron g factor in the vacuum, μ_B is the Bohr magnetron, and $\hbar$ is Plank's constants. For atomic wave functions the expected value of $\frac{1}{r^3}$ is proportional to Z^3. We therefore find:

$$H_{SO} \propto Z^4 (\mathbf{S} \cdot \mathbf{L}) \tag{1.3}$$

This indicates that the strength of the SOC is proportional to Z^4, and is dependent on the interaction between the electrons spin state and the electron momentum. When the electron approaches a nucleus there is a gradient in the magnetic field experienced by the electron due to this SOC. This creates a force $\mathbf{F} = -\nabla(\boldsymbol{\mu} \cdot \mathbf{B})$, where the direction of $\mathbf{F}$ is dependent on the sign of the spin. This is the principle for Mott scattering, which is the basis for one skew scattering, a mechanism of the Spin Hall Effect.

The Hamiltonian for spin-orbit coupling can be written more generally, for both solids and vacuums, as

$$H_{SO} = \lambda_{SO}^{eff} \boldsymbol{\sigma} \cdot (\mathbf{k} \times \boldsymbol{\nabla} V(r)) \tag{1.4}$$

where σ is the Pauli spin matrix, $\mathbf{k} = \frac{\mathbf{p}}{\hbar}$, and $V(r)$ is the potential corresponding to the electric field of the nucleus. λ_{SO}^{eff} is the spin-orbit coupling constant, which is defined as:

$$\lambda_{SO}^{eff} = \frac{P^2}{3E_g^2}[1 - (1 - \xi)^2] \tag{1.5}$$

where $\frac{m_0 P^2}{\hbar^2}$ is approximately the atomic Rydberg energy of the material, E_g is the energy gap, and $\xi = \frac{\Delta_{SO}}{E_g + \Delta_{SO}}$. Δ_{SO} is a energy from the splitting of degenerate states due to the SOC. From this relation it is possible to see that the important intrinsic properties of the material for determining the strength of the SOC are the atomic number Z and the band structure.

1.1.2 Rashba SO Coupling

Rashba Spin Orbit Coupling is found in crystals lacking an inversion center leading to the spitting of the electronic energy bands [12]. This is the basis for the intrinsic mechanism, which will be discussed later. Rashba SOC can be described by the Hamiltonian [3, 7]:

$$H = \frac{p^2}{2m} - \frac{\lambda}{\hbar} \boldsymbol{\sigma} (\hat{z} \times \boldsymbol{p}) \tag{1.6}$$

where λ is the Rashba Coupling constant, m is the mass of the electron, $\hat{z}$ is perpendicular to the plane, and p is the momentum. Therefore, the factors that affect the

strength of Rashba SOC are the direction and magnitude of the momentum, and the Rashba coupling constant, which is material dependent. This Hamiltonian describes the magnetic field that is created by the potential within the crystal, leading to SOC in between scattering events.

1.2 SHE Theory

In 1879 Edwin Hall discovered that in the presence of a magnetic field a conductor develops a transverse voltage due to the Lorentz force. He later realized that in a FM this voltage is dependent on the external magnetic field and the magnetization of the FM [6]. This effect is known today as the Anomalous Hall Effect (AHE). The AHE occurs when a charge current through a FM creates a transverse charge current with opposite directions for the different spin polarities. The asymmetric deflection of the charge current is due to the spin-orbit coupling of the FM. Since FM charge currents normally have a polarization, this will result in a net transverse charge current.

Dyakonov and Perel predicted the extrinsic Spin Hall Effect(SHE) in 1971 based on the theory for AHE[3, 13]. The SHE was not explored further until the early 2000s, when use in the emerging field of spintronics was realized [3]. The SHE was first experimentally observed in 2004 [14]. In 2012 a Giant Spin Hall effect (GSHE) was found in $\beta-$Ta [15]. Since then a GSHE has been observed in $\beta-$W and $\beta-$Pt [1].

The SHE is similar to the AHE in that spin-orbit coupling causes the charge current to be deflected and accumulate on the edges. However NM materials are unpolarized so there exists the same number of spin up and spin down electrons. After deflection there will be an equal number of electrons on either edge of the material. Therefore there will not be a transverse charge current[3]. However, the opposite edges will be polarized differently, creating a spin current.

The process by which charge current is converted to the transverse spin current is described by $J_s = \Theta_{SH}(\hat{\sigma}$ x $J_c)$ where $\hbar J_s/2e$ is the spin current density, J_c is the charge current density, and $\hat{\sigma}$ is the spin momentum. $\Theta_{SH}=|J_s|/|J_c|$ is the spin Hall angle (SHA) and is a measure of conversion efficiency [9]. The SHA is the most commonly used parameter to describe the magnitude of the SHE in a material.

The SHE, and other spin dependent Hall effects including AHE and Inverse Spin Hall Effect (ISHE), have both intrinsic and extrinsic contributions. The intrinsic contribution to the SHE occurs in between scattering events. The spin-orbit coupling of electrons with the virtual inner band transitions of the material leads to the spin-dependent deflection. The strength of the SHE due to intrinsic contributions is dependent on the electronic band and is proportional to the spin-orbit polarization at the Fermi level [3, 6].

Extrinsic mechanics for producing a transverse spin-dependent velocity are due to spin-orbit coupling during scattering of electrons. Scattering events can have ex-

trinsic origins, for example impurities or grain boundaries, or intrinsic origins such as phonons. The extrinsic mechanisms are skew scattering and side-jump. Skew scattering arises from spin-orbit coupling generating a spin-dependent force as explained in Section 1.1. Due to the effects of skew scattering, the momentum of the electron after scattering is dependent on the spin [3]. Skew scattering is not reliant on symmetry breaking from for example added impurities, crystal anistropies, or an external magnetic field [6]. The side jump arises from the the scattering of the Gaussian wave packet off of spherical impurities. This results in spin-dependent displacement after repeated collisions due to spin-dependent acceleration or deceleration. The SHA due to side jump increases with the concentration of impurities and is not normally the largest contribution [3, 6].

Because of the complexity of the band structure of metals and transport properties as well as spin decay, simple models are not capable of obtaining spin Hall angles in specific ways [3, 8]. Therefore, much of the research relies on experimentation.

1.3 Material Characteristics

There are several material characteristics that contribute to the strength of the SHE in a material or are relevant to the usefulness of the material in spintronic applications. Du, Wang, Yang, and Hammel(2014) [16] propose three characteristics that can cause the SHE in a transition metal: atomic number, d-electron count, and magnetic ordering. These characteristics, as well as several others, are studied in this thesis.

1.3.1 Atomic Number(Z)

As mentioned above, contributions to the SHE are due to spin-orbit coupling(SOC) during the scattering of electrons or with the virtual inner band transitions between the scattering events. Therefore the SHA can be considered to be a measure of the SOC. It is thought that SOC varies by Z^4[16, 11] for scattering events, which was derived in Section 1.1. It follows that if the extrinsic mechanisms dominates, the SHA would also vary by Z^4 and the SHE would only be prominent in heavier elements.

Several groups have found 3d transition elements to have SHAs comparable to some of the SHA of 5d transition metals, which would not be expected from contributions due to scattering events. [5, 16, 17]. In addition, the differences in SHA expected from the atomic number contribution, is not seen. For instance W is found to have the highest SHA, yet it is not the largest element studied.

According to the intrinsic mechanism the crystal structure plays a role in determining the strength of the SHE. However, the largest SHAs have been found in the 5d series. Determining the relation between the SHA and the atomic number is useful for deciding what materials should be studied as well as studying the dominant mechanism in different materials.

1.3.2 Fullness of orbital

The electronic band structure has a large influence on the SHE in various metals. The intrinsic spin Hall conductivity is proportional to the spin-orbit polarization at the Fermi level, and it has been theorized that the extrinsic mechanisms are proportional as well. Following Hund's rule the spin Hall angle is expected to be positive when the shell is more than half full or negative if the shell is less than half full. In addition, the SHE will be relatively small when not filled, half-filled, or completely filled [6]. Du et all[16] calculations of the SHA for the 3d series confirmed this, with a large negative SHA for Cr and a large positive SHA for Ni.

In transition metals the d-electron count has been found experimentally to have a large effect on the SHE, and large SHAs, comparable to the 5d heavy metals, have been seen in 3d light metals [3, 5, 17]. This is in contrast to the Z^4 expected from SOC due to scattering events. The SHE's magnitude dependence on the fullness of the orbital is not limited to the d orbital. f-electron systems have larger angular momentum then d-electron series and the intrinsic contribution arising from Hund's rule would suggest that the f-electron series could have a strong SHE. [18] Reyonds et all[19] found that the spin torque ratios of the f-series are comparable to those of Ta, Pt, and W; however, the conductivities are significantly lower. More studies into the 3d and f systems with the possibility of tuning using alloys could be new avenues for the SHE.

1.3.3 Spin diffusion length

The spin diffusion length (SDL) describes the decay of the spin current relaxation due to spin-flipping[10]. In a material, there are collisions between electrons and other particles. There are both spin-direction conserving and spin-direction flipping types of collisions [20]. The spin-flipping collisions can be with magnons, phonons, etc [21]. The spin diffusion length is the mean diffusion between spin-flipping collisions [20].

When applying a perpendicular current, a finite spin diffusion length, as opposed to an infinite diffusion length, generally reduces the magnitude of the magnetoresistance(MR). However, increases in MR with a finite SDL have been theorized, especially for materials with thicknesses of a few nm.[20].

A smaller diffusion length is not ideal for several reasons. When the SDL is on the order of a few nm, it is not possible to use "spin manipulation tools along the NM transport channel" [3]. It also constrains the size of the spintronic application due to the decay of the spin current [22]. In addition, a smaller SDL is correlated with a larger resistance, due to the increase scattering events for both phenomena.

The spin diffusion also has a direct influence over the strength of the spin Hall effect. The general relation is: [17]:

$$\frac{\Theta_{SH}(t)}{\Theta(\text{inf})} = \frac{cosh(d/\lambda_s) - 1}{cosh(d/\lambda_s) + R} \tag{1.7}$$

where R is the interfacial condition. Some sources assume R= 0, reducing this relation to [9, 23]:

$$\frac{\Theta_{SH}(t)}{\Theta(\text{inf})} = 1 - sech(\frac{t_{NM}}{\lambda_s}) \tag{1.8}$$

This relationship would suggest that the SHA increases with thickness until within a few factors of the SDL, when the SHA saturates. Studying the spin diffusion length more thoroughly especially in relation to thickness will provide more information about the actual effect. The spin diffusion length is an important parameter due to the relationship with the SHA and its importance in determining the usefulness of a material in applications.

1.3.4 Thickness

The thickness of a material affects several parameters including the stability of the structure and the resistivity. [24, 23, 25]. The thickness with the maximum SHE is also dependent on material characteristics including the spin diffusion length and the relative strengths of the bulk SOC and the surface SOC.

Our group [23] found that beyond a critical thickness (t_c) the lattice constant of the W sample changes from the β structure to the α structure. The α structure has a much smaller resistivity and SHE, and other sources provide support that the material thickness has an influence on the crystalline structure [26]. For materials with this effect, the size of the application is constrained.

For Au, resistivity is negatively correlated with the thickness of the material. At very low thicknesses (5 nm), surface scattering becomes dominant and the resistance increases significantly [24]. For a thin film where the thickness is much greater than the effective electron mean free path the resistivity is predicted to be inversely proportional to the material thickness. This relationship is given by[23]:

$$\rho(t) = \rho_B + \frac{3}{8}\frac{\lambda_{eff}}{t} \tag{1.9}$$

where ρ_B is the bulk resistivity, λ_{eff} is the effective electron mean free path, and t is the thickness. Therefore, for spintronic applications, we would want larger thicknesses with a large SHA in order to increase efficiency.

The optimal thickness is also dependent on the spin diffusion length as shown in equation 1.7. The spin Hall effect is expected to be strongest when the thickness is greater than the spin diffusion length and will increase before stabilizing as described in the previous section.

1.3.5 Resistivity

The resistivity of a material is an important parameter when considering the SHE. High resistivity limits the current density and the resulting spin transfer torque on

the FM.[27] Very high resistivities are impractical for spintronic applications due to the large currents needed and the lower lifetime. However, resistivity is often correlated with a larger SHE. It has been found that the materials with the highest SHA including W, Ta, and Pt all have fairly large resistivities. Going forward, it is important to find materials with smaller resistivity.

Resistance arises from the collision of electrons with particles. However, these scattering events also generate the SHE and are important to SOC. Typically the SHE due to the intrinsic mechanism and side jump is proportional to the resistivity [27].

Many new advances in the SHE are also relying on alloys or impurities, see Section 1.3.7. While this could contribute to larger SHE it is necessary to study the associated increase in resistivity. It has been found that the resistivity of a compound generally increases with impurities [13, 27]. One solution explored in the literature is starting with Au, a material with a small SHE and small resistivity, and doping it with Ta, which has a higher SHA and resistivity. This produced a alloy with a SHA comparable to W, but with a smaller resistivity [27].

1.3.6 Temperature

The temperature dependence of properties fundamental to the SHE is important for characterizing the material. Specifically, the dependence of the SHA on temperature provides insight into the dominant mechanism contributing to the SHE [3, 28]. For example, it is expected that if the intrinsic contribution is dominant, then the spin Hall angle will increase linearly with temperature [29]. In addition, it is necessary for applications that the SHE does not vary significantly with temperature.

1.3.7 Alloys and impurities

A recent area of research interest in the SHE has been studying alloys and impurities. Past studies have shown that it is possible to tune the spin Hall angles through increasing the strength of the extrinsic mechanisms by changing the host and impurity combination or ratio [13, 30].

Theoretically, the magnitude of the SHE due to skew scattering is dependent on the contrast between SOC of impurity and host and the magnitude of the side jump is proportional to the impurity concentration [3, 6]. Therefore, both of these mechanisms are highly tunable through impurities.

However, the mechanism being strengthened must provide a large contribution to the SHE in the given structure. It has been found that when a host has a large spin-orbit interaction, for example Pt, the variations due to impurities are suppressed, while for Cu and Au which have weaker spin-orbit interactions, there is a much larger variation in the spin Hall angle depending on impurity. In addition, the contributions to the SHA of the impurity and the host, or the two materials in an alloy can actually

work against each other, decreasing the total effect [22, 27].

It has been found in several systems that resistivity of a compound increases with impurities, and the relationship can be linear[13, 27]. Large resistivities are impractical in spintronic applications, and their presence must be studied in addition to the SHA.

Alloys also provide the possibility to create materials with longer diffusion length and a large SHE, which is highly desirable. Gradhand, Fedorov, Zahn, and Mertig [22] were able to tune the SDL by creating impurities in Cu, Au, and Pt. Using this method, they noticed that the largest SDL had a large SHA as well, which is due to small longitudinal conductivity.

Chapter 2:
Experiment

2.1 Fabrication

We deposited a series of multilayer stacks on thermally oxidized Si wafers in a home-made high vacuum magnetron sputtering system. The thin-films were patterned using photolithography into standard Hall bars(20 x 55 μm^2), as shown in Figure 2.1, for both Hall effect and resistivity measurements.

Before measurements, the patterned samples were annealed in vacuum(1 x 10^{-6} Torr) at different temperatures and with a magnetic field of 0.45 T perpendicular to the sample planes. The temperature was ramped up over the course of 2 hours and 40 minutes using the following sequence: ramp(20 min), dwell(20 min), ramp(20 min), dwell(20 min), ramp(10 min), dwell(10 min), ramp(10 min), dwell(10 min), ramp(10 min), dwell(10 min), ramp(5 min), dwell(5 min), ramp(5 min), dwell(5 min). Over each ramping period the temperature rises approximately half of the value needed to get to the final temperature. Once at the final temperature the sample is annealed for 2 hours. The system is then naturally cooled over the course of 6 hours.

The annealing temperature is chosen to produce the best perpendicular magnetic anisotropy (PMA). When a FM has magnetic anisotropy there is an energetically favorable "easy axis" and in the absence of an external magnetic field the magnetization will align with one of the two directions along the axis. If the FM has PMA, the easy axis is aligned perpendicular to the FM-NM interface. To measure this we apply a magnetic field perpendicular to the bilayer. If the sample has PMA, we only expect to see two magnetizations which will alternate depending on whether the applied magnetic field is positive or negative.

To measure the PMA, the sample is mounted on a holder and wire-bonded in the pattern to measure Hall resistance as shown in Figure 2.1(a). We then apply a current of a few mA to the system and the resistance is measured for a range of magnetic fields, generally from -100 G to 100 G. We expect to see a distinct 2 state sample, such as ones shown in Figure 2.2, where the resistance changes between the high and low states instantaneously. By changing the final ramping temperature and the dwell time, we are able to fine tune the PMA.

We are able to measure the resistivity of the material by bonding the sample as shown in Figure 2.1(b) and using the relation $R = \rho\frac{l}{S}$. This is important for calculating the SHA and for characterizing the phase of the sample. For instance, α-W has a much lower resistivity than β-W.

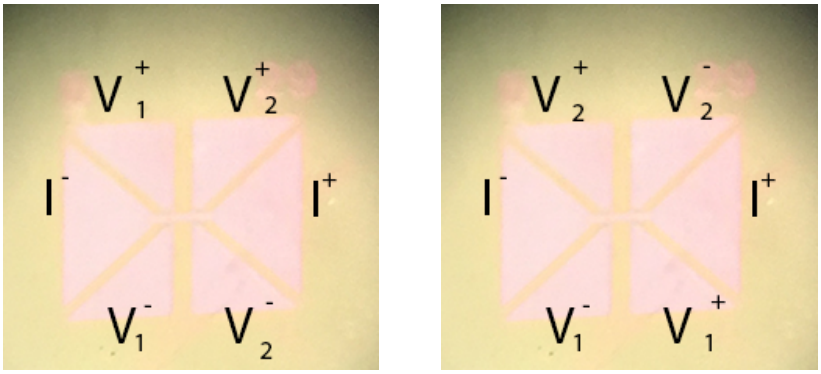

(a) (b)

Figure 2.1: The Hall Bar used for measuring the Hall resistance (a) and the resistivity (b) of a material. In either set of measurements, it is possible to use the first set of voltages or the second set of voltage.

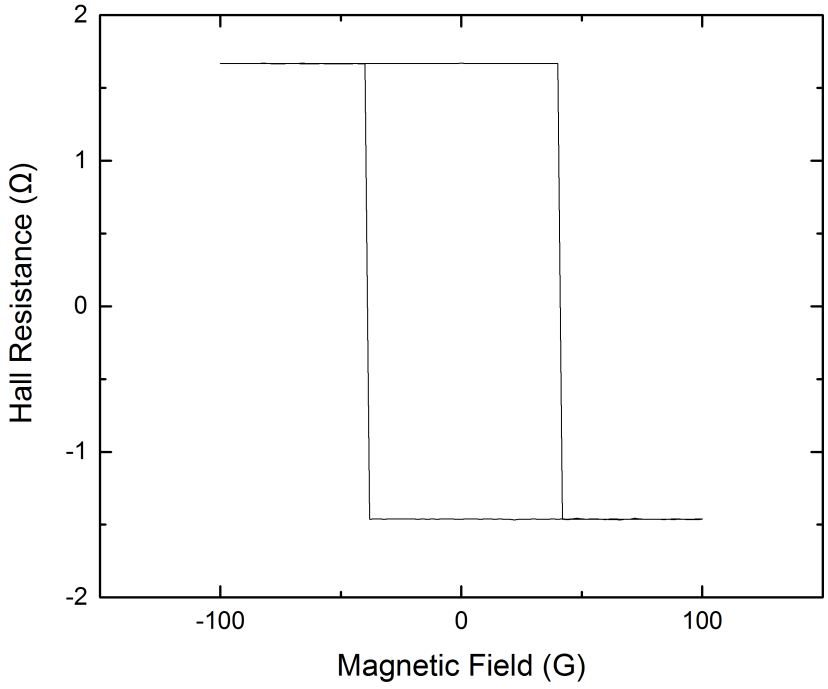

Figure 2.2: Measured PMA for Ta sample annealed at 200 K as described in section 2.1

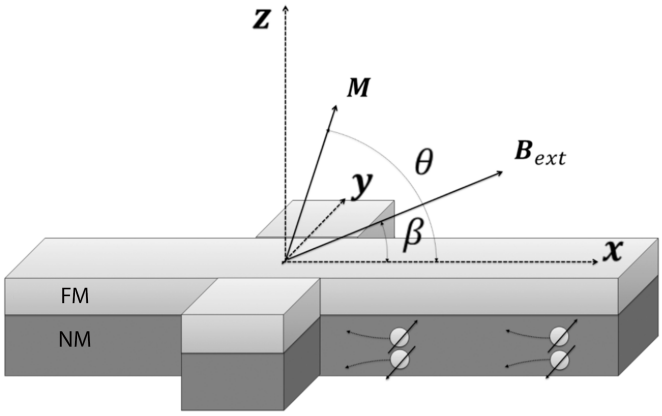

Figure 2.3: Diagram of the experimental procedure used to measure the Spin Hall Angle. A current is applied along the x axis and a voltage is measured along the y axis. Adapted from [1]

2.2 Measurement

We perform magneto-transport measurements on these stacks using the Quantum Design Physical Property Measurement Systems (PPMS). The conditions for the magneto-transport measurements are shown in Figure 2.3. We apply an external magnetic field (B_{ext}) in the y-z plane at an angle β from the y axis, where we attempt to make β close to 0. We send in a direct current along the y axis of the Hall-bar sample and measure the Hall voltage along the x-axis. The resulting magnetization vector(M) is in the y-z plane at an angle θ from the x axis. The direction of M is determined by B_{ext}, the spin-transfer torque(STT) from the spin current and internal magnetization conditions.

We measure the Hall resistance with both a positive and negative charge current, for a variety of currents, over a range of B_{ext} such that M rotates from 90° to 0°. The curves for the Hall resistances with an applied current of ± 4 mA and an external magnetic field varied from 0 to -10000 G are shown in Figure 2.4(a). The difference in the curves is due to the torque exerted on the FM layer by the spin current.

To perform the calculations, we must also determine the value of β in the system. Theoretically to do this we can use the relation $H_C = B_C \sin\beta$, where H_C is the value of B where switching occurs when applying a perpendicular magnetic field, and B_C is the value of B where switching occurs when applying B_{ext}. When performing these measurements we found that B_C can vary significantly yielding very different values of β. For our calculations we often used the value of β that yielded the most linear relationship between the spin transfer torque and the $B^+ - B^-$ as discussed in the analysis.

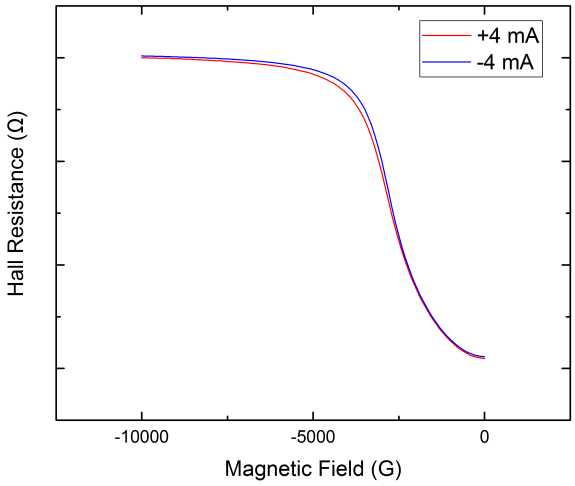

(a)

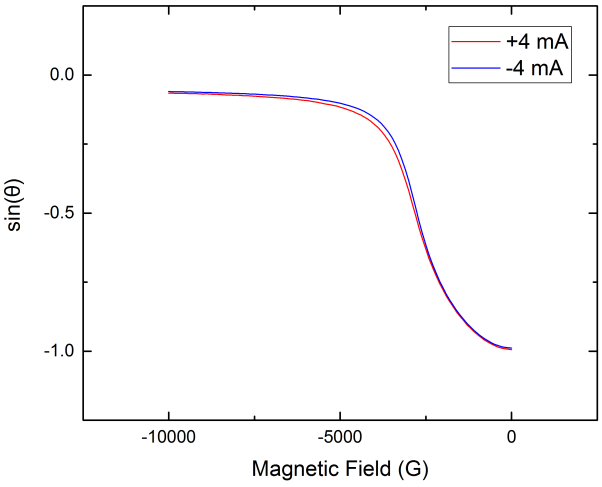

(b)

Figure 2.4: Ta sample annealed at 200 with magnetic field applied according to diagram 2.3 where $\beta \approx 2.25$. Figure (a) shows the raw data. The difference in the Hall resistance for the positive and negative curve is due to the SHE. (b)The Hall resistance measured is transformed into $\sin\theta$ as described in section 2.3.

2.3 Analysis

The systems used to measure the resistances both to determine PMA and to determine θ often have other points or resistance beyond what we want to measure. The two-states seen in the PMA measurements, R_{0high} and R_{0low} should be equal and opposite, but generally there exists an offset. To account for this, we can normalize the data from Figure 2.4(a) by $\frac{R_H+R_{0high}+R_{0low}}{R_{0high}-R_{0low}}$, which converts the measured hall resistance into sinθ as shown in Figure 2.4(b). To determine the SHA, we consider the equilibrium condition for M which is [25]:

$$\tau_{tot} = \hat{x} \cdot (\vec{\tau}_{ST} + \vec{\tau}_{ext} + \vec{\tau}_{an}) = \tau^0_{ST} + B_{ext}\ \sin(\theta - \beta) - B^0_{an}\ \sin\theta\ \cos\theta = 0 \qquad (2.1)$$

where $\tau^0_{ST} = \frac{\hbar}{2eM_st} J_s$ is the spin-transfer torque due to the spin current J_s, τ_{ext} is the torque on the magnetization due to the external magnetic field. and τ_{an} is the torque due to the perpendicular anistropy field. Since we measured the resistance for both a positive and negative charge current, at a given θ two B_{ext} values exist, $B_+(\theta)$ and $B_-(\theta)$. The magnetic field breaks the symmetry of the high and low states, such that one rotation direction is preferred. Therefore, for a positive magnetic field one spin current will work the magnetic field and one spin current will work against it. From equation 2.1 we find,

$$\tau^0_{ST}(+J_s) + B_+\ \sin(\theta - \beta) - B^0_{an}\ \sin\theta\ \cos\theta = 0 \qquad (2.2)$$

$$\tau^0_{ST}(-J_s) + B_-\ \sin(\theta - \beta) - B^0_{an}\ \sin\theta\ \cos\theta = 0 \qquad (2.3)$$

By subtracting equation 2.3 from equation 2.2, and given that $\tau^0_{ST}(+J_S)$ -$\tau^0_{ST}(-J_S)$ $= 2\tau^0_{ST}(|J_S|) = \Delta\tau^0_{ST}$, we obtain:

$$B_+(\theta) - B_-(\theta) = \Delta\tau^0_{ST}/\sin(\theta - \beta) \qquad (2.4)$$

We then plot $B_+(\theta) - B_-(\theta)$ versus $\sin(\theta - \beta)$ to obtain τ^0_{ST}. Since the data for B_+ and B_- will have slightly different values for $sin\theta$, we have to choose one set of $sin\theta$ to find θ and to construct the graph. Then we must interpolate the other data set to these new values. There are several programs to do so, one used is the table formula in kaledigraph. Several different values of β were used when plotting the graph. The value of β that resulted in the most linear relationship between $B_+(\theta) - B_-(\theta)$ and $\sin(\theta - \beta)$ was used in further calculations.

We create each of these plots for several currents, generally in the range 1-4 mA as shown in Figure 2.5(a). We then plot $\Delta\tau^0_{ST}$ vs the applied current, as shown in Figure 2.5(b) so that we are able to find a more accurate Θ_{SH}.To find the value of the SHA, we can use the formula,

$$\Theta_{SH} = J_s/J_c = \left(\frac{2eM_st}{\hbar}\right)(\tau^0_{ST}/J_C) \qquad (2.5)$$

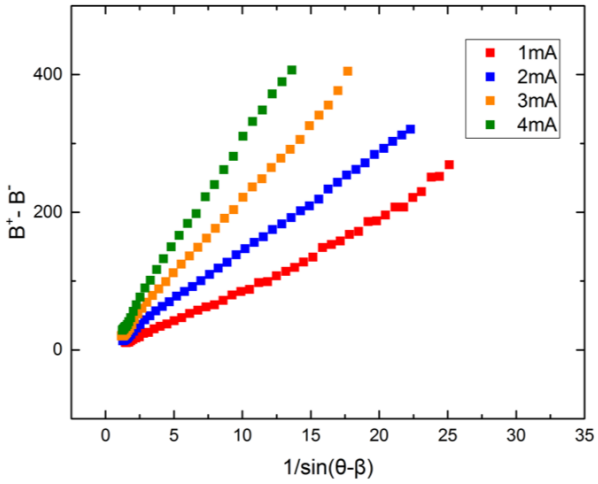

(a)

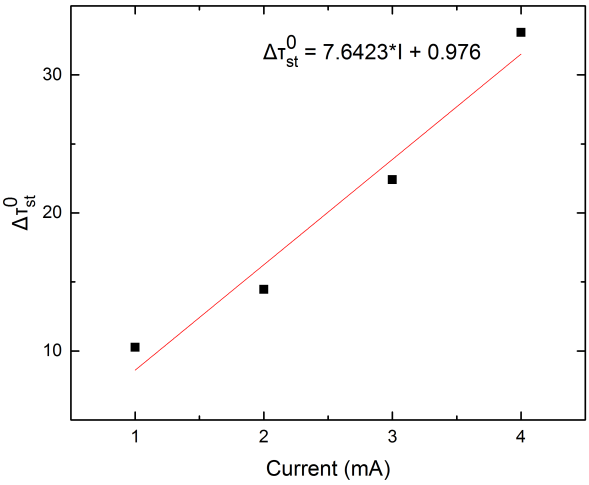

(b)

Figure 2.5: Ta sample annealed at 200 with magnetic field applied according to diagram 2.3 where $\beta \approx 2.25$. (a) Linear relationship between $B_+(\theta)$ - $B_-(\theta)$ and $1/\sin(\theta - \beta)$ as described by equation 2.4 for currents between 1 and 4 mA. (b) $\Delta\tau^0_{ST}$ as a function of the applied current.

where M_s is the spontaneous magnetization of the material we are studying, t is the thickness of ferromagnetic layer, τ_{ST}^0 is the spin transfer torque found above, and J_C is the charge current density through the material we are studying. To find J_C we must know the resistances of each material to determine how much of the charge current applied goes through the material of interest. We then use the dimensions of the sample to find the density. More details about the experimental procedures and analysis our lab does can be found in our past works [23, 25, 28].

When performing the analysis there are several difficulties that we commonly encounter when trying to calculate Θ_{SH}. At low magnetic fields it is fairly common to encounter switching between the high and low states due to the current, especially when larger currents are applied.In addition, as θ approaches 0° or 90°, the differences in the Hall resistance for a positive or negative current often are negligible, leading to difficult analysis and only a small number of usable data points.

In addition, in one Ta sample, we observed that the STT exerted by the negative current worked with both the positive and negative magnetic field to bring the magnetization from $\pm 90^\circ$ to 0°. A more in depth study of the different torques, as well as the broken symmetry exerted by the magnetic field is necessary to explain this phenomenon.

Chapter 3:

Results

The results of the work in our lab and various other lab groups are analyzed in the following section. The data with their sources are listed in appendix A.

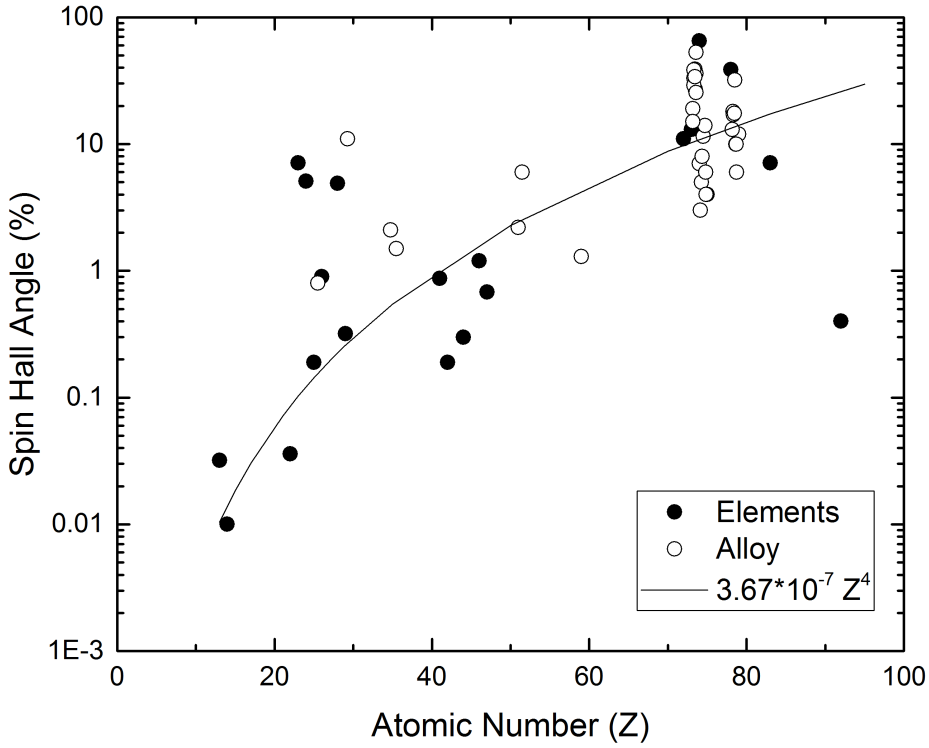

Figure 3.1: The spin Hall angle as a function of the atomic number for pure elements (closed circle) or the effective atomic number for alloys(open circle). The effective atomic number for the alloys was found by averaging the components based on their concentrations.

We first studied the relationship between the atomic number and the SHA, the results are shown in Figure 3.1. For each material the largest experimentally found value was used. As shown in the graph, the relationship between SHA and the atomic number is approximately proportional to Z^4 as predicted by theoretical relationship between SOC and Z from section 1.1.

However, this relation only gives the general trend and there are several notable exceptions. There are a group of elements where Z is between 20 and 30, where there

is a large variation in SHA and the SHA is comparable to the SHA of the 5d elements. These are the 3d elements, and the trends surrounding the difference in SHA for the transition elements are discussed below. What is notable is that the 3d elements with the weaker SHA follow the Z^4 relation, while the strong SHE 3d elements are much larger. This confirms what Du et all [16] stated, that the factors influencing the SHA are additive not multiplicative.

This however does not seem to hold for non-transition elements. For instance uranium, shown in this graph with Z = 92 has a SHA on the order of elements with an atomic number between 40 and 50.

The SHA varies much more for alloys. There is a series of materials with an effective Z between 78 and 79, which corresponds to Au(x)Pt(1-x) alloys, where x various from 0 to 1. As can be seen, alloys allow for much more significant tuning of the SHA for similar effective Z's.

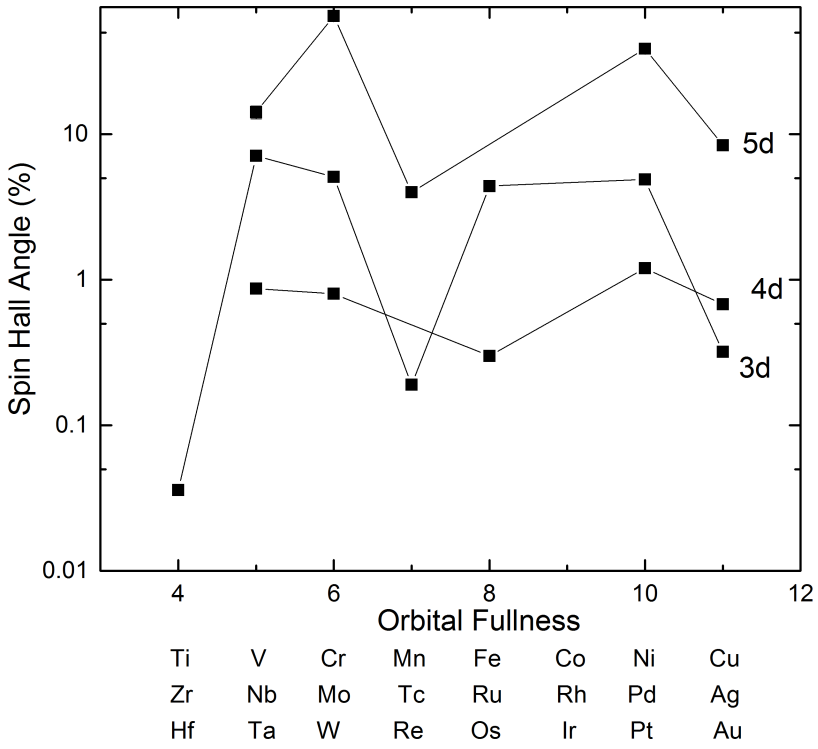

Figure 3.2: The spin Hall angle as a function of the n value for the 3d, 4d, and 5d transition metals. The n value is the fullness of the respective d orbital and the following s orbital

Figure 3.2 shows the relationship between the magnitude of the SHA and the orbital fullness for the transition metals(d-series). The orbital fullness (n) is defined as the number of electrons in the d orbital and the following s orbital, which is the standard used in the literature [6, 16]. It also corresponds to the group of the periodic

table in which that element resides. For all three series, the magnitude of the SHE is largest when the d-orbital is approximately a quarter full or three-quarters full, which is the relationship that we expected to see. This relation arises from the intrinsic spin Hall effect, which depends on the Fermi surface of the material.

What is not expected is that the 4d elements have a smaller spin Hall angle than the corresponding 3d elements. This is likely because the 4d elements have not been studied in depth and experimental values for the same element have been known to vary more than an order of magnitude. For instance, values for Au range from 0.335 to 12 [3]. In addition, the 3d and 4d series contain more elements within the series that have relatively large SHAs compared to the rest of the series. In the 5d series, the SHAs of W and Pt are significantly larger than the surrounding elements. Based on the 3d and 4d trends we would expect the SHA of Ta to be much larger. It is also possible to see that the minimums in the series occur at different values of n. In the 4d series it occurs at n = 8 for the SHA of Ru, while for the 3d series, the SHA of Fe, also n = 8, is fairly large. The local minimum spin Hall angle for the 3d and 5d both occur at n = 7. This differences could be explained by variability in experimental techniques and theoretical approximations or the lack of data. While the values for the SHA for the 3d elements came from the same group, the values for the 4d and 5d elements came from a variety of labs and experimental techniques. The differences might also arise from fundamental mechanisms not considered here.

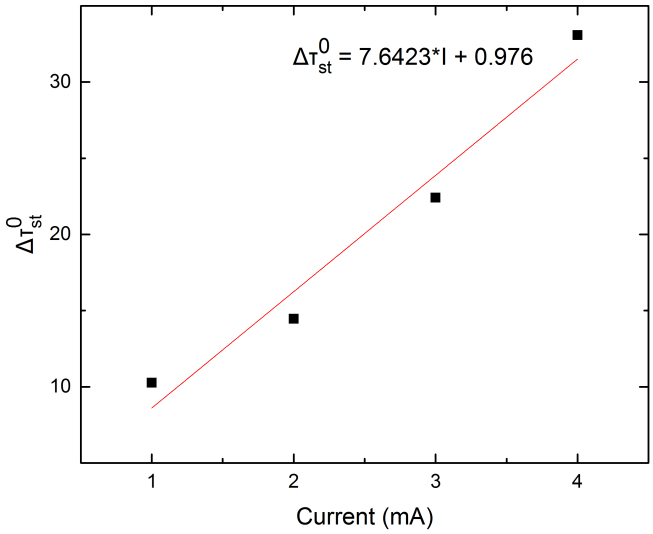

Figure 3.3: The Spin Hall Angle as a function of the thickness of the NM layer. Each material's SHA measurements were performed by the same group.

As can be seen in Figure 3.3, the dependence of the Spin Hall Angle on thickness

various significantly, especially with regard to the spin diffusion length. While the SHAs for Pt, V, and Au saturate shortly after the thickness of the layer surpasses λ_s, the SHA for W continues to increase following λ_s. In addition, the SHA for V increases until it reaches λ_s, while the SHA for Au decreases. There are several material dependent parameters that could influence the SHA including resistivity due to surface scattering, spin current transmission along the interface, and the bulk spin Hall angle.

One of the main contributions is expected to be the relative strength of the surface SOC and the bulk SOC. Au likely has stronger SOC on the surface, so the spin Hall effect is most efficient when the film is thin. Ta has stronger bulk SOC, so as the bulk increases, so does the spin Hall angle. Given these results, Au might be better used as a 2d material, while W would be used for applications that require thicker layers.

The spin diffusion length (λ_s), the resisivity (ρ), and Θ_{SH} all are dependent on the number of scattering events, so they were analyzed together in Figure 3.3. The λ_s is the average distance an electron travels before its spin flips. So, even though an electron might collide 10 times, it might only have its spin flip once. There is still a relation to the number of collisions the electron experiences. On average, the more collisions, the shorter λ_s. ρ is also related to the number of collisions, the more collisions the larger the ρ is. The spin Hall effect intrinsic and side jump mechanisms also increase with the number of scattering events [27].

We therefore would expect the ρ to be somewhat proportional to the θ, since both increase with more collisions, while the λ_s is expected to be inversely proportional to both Θ_{SH} and ρ. Ideally however, we want a material with a large Spin Hall angle, a large spin diffusion length, and a small resistivity.

Figure 3.4(a) shows the spin diffusion length(λ_s) as a function of the resistivity(ρ). There is a clear negative correlation between the ρ and λ_s as expected. However, there were several materials with a very large λ_s and ρ. This likely occurs in materials where the number of scattering events that are spin flipping are very low. Figure 3.4(b) shows that there is also a negative correlation between Θ_{SH} and λ_s as expected. The largest Θ_{SH} occur when the λ_s is fairly small, on the order of 1-20 nm. However, there exists a set of measurements with moderate Θ_{SH} and a larger λ_s. The particular materials' Θ_{SH} as a function of resistivity, shown in Figure 3.4(c), suggest that these measurements were from Au samples.

While W and Ta are both well studied and have large SHAs, their resistivity is fairly large (over 100 $\mu\Omega$*cm), which does not make them ideal candidates for spintronic applications. Au has a consistently lower resistivity then the other elements studied while having a moderate SHA. AuW and AuTa alloys are also studied. The AuTa alloys reach a SHA of about 50%, which is much larger than the SHA of Ta or Au, while having a resistivity slightly lower than TA. This suggests with the right combination the resistivity can be lowered.

For each particular material there does not appear to be a particular trend suggesting that it might be possible to tune the resistivity for a given material independently

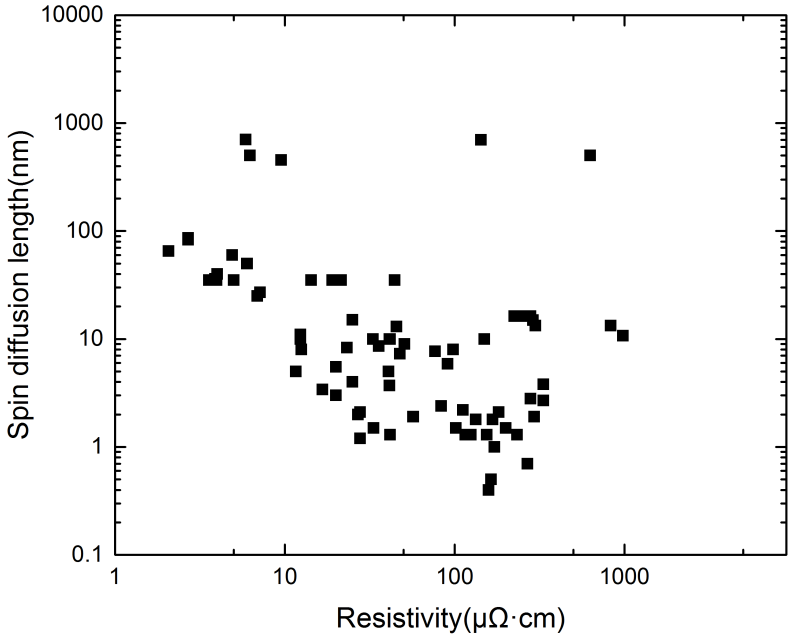
Spin diffusion length(nm)
10000
1000
100
10
1
0.1
1
10
100
1000
Resistivity(μΩ·cm)

(a)

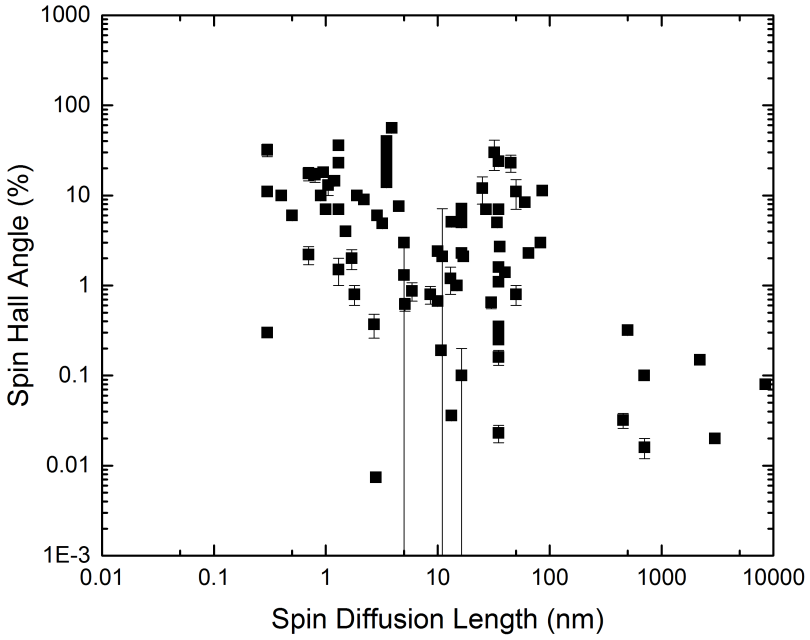
Spin Hall Angle (%)
1000
100
10
1
0.1
0.01
1E-3
0.01
0.1
1
10
100
1000
10000
Spin Diffusion Length (nm)

(b)

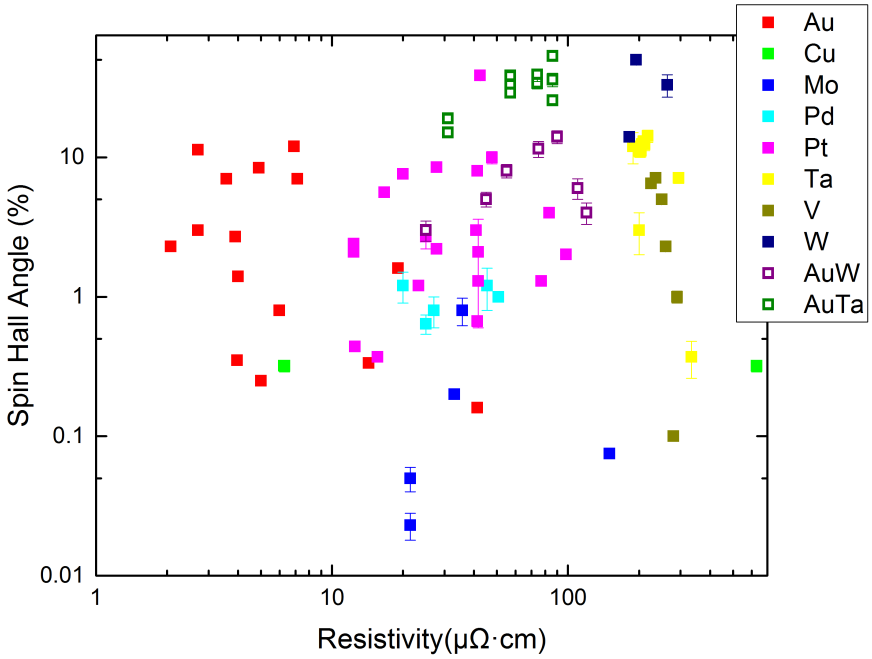

(c)

Figure 3.3: (a) The spin diffusion length as a function of the resistivity. (b) The spin Hall angle as a function of the spin diffusion length. For both (a) and (b) The data set includes multiple measurements from the same material. (c) The spin Hall angle as a function of the resistivity for several different materials, each colored differently. Closed squares are elements, while open squares are alloys.

of the spin Hall angle. Examining the entire data set, the alloys generally have larger SHAs at a given resistivity. This suggests that alloying might be useful in spintronic applications in order to tune the resistivites and spin diffusion lengths.

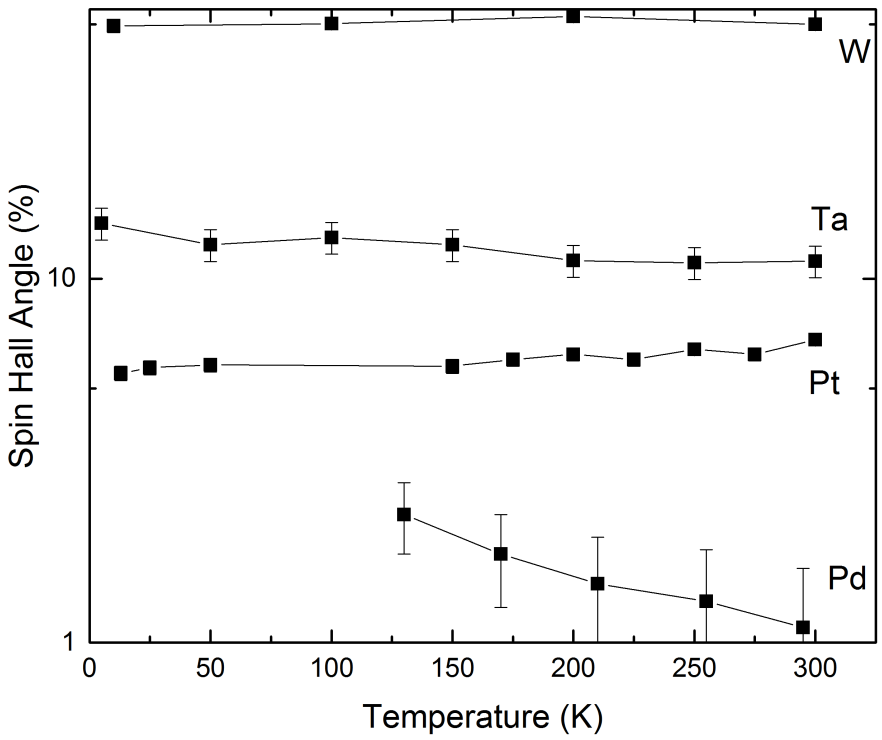

Figure 3.4: The spin Hall angle as a function of the temperature for several elements. Each material's SHA measurements were performed by the same group.

Figure 3.4 shows the Spin Hall Angle as a function of temperature for several materials. None of the Spin Hall Angles vary much in absolute value over the temperature range, however the Θ_{SH} varies for Pd by about a factor of 2. The temperature dependence that are seen show that the SHA for W and Pt increase with temperature while the SHA for Ta and Pd decrease with temperature. From the temperature dependence studies it was determined that in Ta the dominant mechanism is the extrinsic skew jump [1] while for Pt the intrinsic mechanism was determined to be dominant [9]. This difference explaining the opposite dependence on temperature. In addition, it supports the theory from 1.3.6 that if the intrinsic mechanism is dominant the spin Hall angle increases with temperature. What is surprising is that Pt and Pd are in the same group, but their SHAs have opposite temperature dependence, and Ta and W are adjacent on the periodic table, but their SHAs also have opposite temperature

dependence [31].

Figure 3.5 plots the spin Hall angle as a function of the spin Hall angles of the components of the alloys, where the smaller SHA of the two components is plotted on the x-axis. From the figure it is evident that the smaller Θ_{SH} out of the components of the alloy has a strong influence over the strength of the SHE in the alloy, with no significant SHAs unless both components have a Θ_{SH} of at least $\sim 10\%$. This suggests that the mechanism contributing to these alloys is not intrinsic. Alloying often result in changes in the lattice structure and we would therefore not necessarily expect to see a dependence on the spin Hall angles of the components.

In addition, when doping, the skew scattering is larger when the strength of the SOC between the host and impurities is larger. Although alloying is on a more macroscopic scale, we might expect to see the same relation.

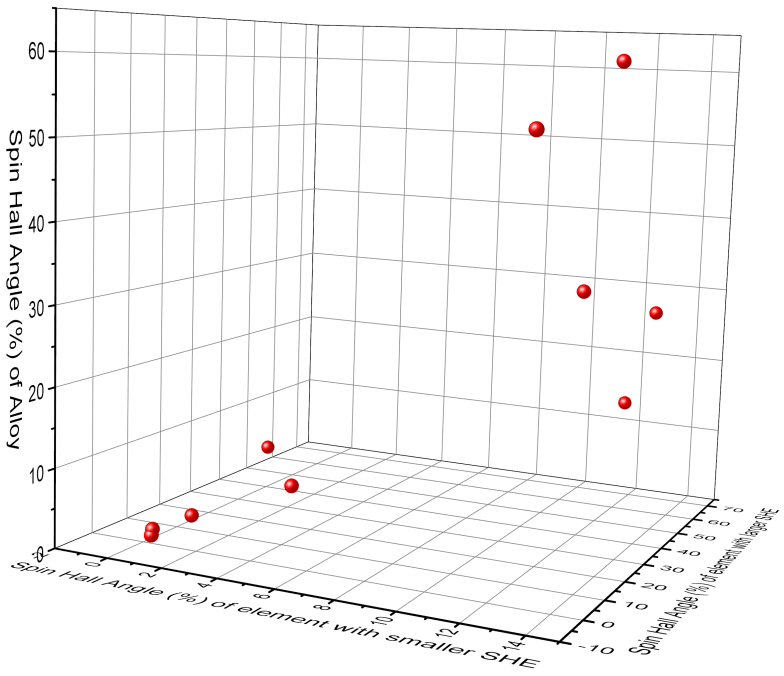

Figure 3.5: The spin Hall angle as a function of the spin Hall angles of the components of the alloys. For each alloy, the component with the larger SHA is plotted on the y-axis. Alloys where one component does not have a recorded spin Hall angle is not included. For alloys systems where the concentrations are varied, only the largest Θ_{SH} is included in this plot

Chapter 4:
Conclusion and Future Work

In this thesis spin Hall angles were studied in relation to various parameters of the materials examined, specifically those that have large influence over the magnitude of the Spin Hall Effect or are important for determining usefulness in spintronic applications. We determined that a portion of the contribution to the spin Hall effect is due to the atomic number and that there is a general trend that Θ_{SH} varies by Z^4. However, it is not the only factor. The other primary factor considered was the orbital fullness leading to differences in the Fermi surface and differences in the intrinsic mechanism. Although some 3d elements did have a relatively large Θ_{SH}, approaching 10%, none of them got close to the Θ_{SH} seen in W and Pt of $\sim 65\%$ and $\sim 38\%$ respectively.

In regards to the orbital fullness, there were some difference in the trends for the 3d, 4d, and 5d series that was not expected. It was expected that the variation due to the orbital fullness would affect each row equally, but it appears that this is not the case. When studying the temperature dependence of Θ_{SH} it was also observed that Pd and Pt had a different dependence even though they are in the same group. This suggests there might be another dependence on the number of electrons that is not considered in this thesis.

We found that the Θ_{SH} dependence on thickness and temperature varied significantly with the material, although only a few materials were studied. For the thickness dependence, all 4 materials studied had different dependencies. Both are important for applications because the dependence on thickness constrains the size of the application, and a large dependence on temperature can create problems for usability.

For spintronic applications, having low resistivity and a large spin diffusion length is ideal. However, for many of the materials that have been studied large spin Hall angles also have large resistivities. Au and Au alloys tend to have larger spin Hall angles for a given resistivity, suggesting these might be key materials to study. Given that Cu is in the same group as Au and is much more abundant, it could be a good material to study as well.

In addition, numerous studies have shown that the resistivities can be tuned by alloying and by varying the concentrations or materials [8, 32, 27] providing avenues for future work. Most of the work involving alloys has been focused on the extrinsic mechanism, and there has not been significant work studying the ability to alter the crystal structure and therefore the intrinsic contribution.

In this report, we did not quantitatively study the crystal structure or impurities in depth; both have been shown to have a large effect on the spin Hall angle. Studying the crystal structure might offer insight on the range in trends for the temperature and thickness dependencies. We also only focused on the magnitude of the spin Hall

angle. Materials can have spin Hall angles of opposite signs, which often vary based on the fullness of the orbital. Studying the alloying of two materials of the same or opposite signs is another avenue for research.

In addition, there are several other parameters that are important to the usefulness of a material in a spintronic application. This includes interfacial diffusion and the strength of the magnetization in the FM layer and how this relates to the choice of NM/FM bilayers; the necessary external magnetic field such that an applied current can create switching; and the feasibility of mass producing the bilayer, including the abundance of the materials.

Overall, very large spin Hall angles have been observed, however they are always accompanied by a large resistivity and a small spin diffusion length, while some moderate spin Hall angles have been found with a lower resistivity and larger spin diffusion length. Going forward, alloys and doping provide a method for tuning parameters to create materials with large spin Hall angles that are also useful in spintronic applications.

Bibliography

[1] Qiang Hao and Gang Xiao. Giant spin hall effect and magnetotransport in a ta/cofeb/mgo layered structure: A temperature dependence study. *Phys. Rev. B*, 91:224413, Jun 2015.

[2] Claude Chappert, Albert Fert, and Fradaric Nguyen Van Dau. The emergence of spin electronics in data storage. *Nature materials*, 6:813–23, 12 2007.

[3] Jairo Sinova, Sergio O. Valenzuela, J. Wunderlich, C. H. Back, and T. Jungwirth. Spin hall effects. *Rev. Mod. Phys.*, 87:1213–1260, Oct 2015.

[4] S.D. Bader and S.S.P. Parkin. Spintronics. *Annual Review of Condensed Matter Physics*, 1(1):71–88, 2010.

[5] R. Yu, B. F. Miao, L. Sun, Q. Liu, J. Du, P. Omelchenko, B. Heinrich, Mingzhong Wu, and H. F. Ding. Determination of spin hall angle and spin diffusion length in β-phase-dominated tantalum. *Phys. Rev. Materials*, 2:074406, Jul 2018.

[6] A. Hoffmann. Spin hall effects in metals. *IEEE Transactions on Magnetics*, 49(10):5172–5193, Oct 2013.

[7] Jairo Sinova, Dimitrie Culcer, Q. Niu, N. A. Sinitsyn, T. Jungwirth, and A. H. MacDonald. Universal Intrinsic Spin Hall Effect. , 92:126603, March 2004.

[8] M. Obstbaum, M. Decker, A. K. Greitner, M. Haertinger, T. N. G. Meier, M. Kronseder, K. Chadova, S. Wimmer, D. Ködderitzsch, H. Ebert, and C. H. Back. Tuning spin hall angles by alloying. *Phys. Rev. Lett.*, 117:167204, Oct 2016.

[9] Xuepeng Qiu Jae Hyun Kwon Hyunsoo Yang. Yi Wang, Praveen Deorani. Determination of intrinsic spin hall angle in pt.

[10] Xinde Tao, Qi Liu, Bingfeng Miao, Rui Yu, Zheng Feng, Liang Sun, Biao You, Jun Du, Kai Chen, Shufeng Zhang, Luo Zhang, Zhe Yuan, Di Wu, and Haifeng Ding. Self-consistent determination of spin hall angle and spin diffusion length in pt and pd: The role of the interface spin loss. *Science Advances*, 4(6), 2018.

[11] Garlid Eric Scott. *Electrical detection of the spin Hall effect in ferromagnet-semiconductor heterostructures.* PhD thesis, Retrieved from the University of Minnesota Digital Conservancy, http://hdl.handle.net/11299/93900., 2010.

[12] A. Manchon, H. C. Koo, J. Nitta, S. M. Frolov, and R. A. Duine. New perspectives for rashba spin–orbit coupling. *Nature Materials*, 14:871 EP –, 08 2015.

[13] Y. Niimi, H. Suzuki, Y. Kawanishi, Y. Omori, T. Valet, A. Fert, and Y. Otani. Extrinsic spin Hall effects measured with lateral spin valve structures. *Physical Review B*, 89:054401, February 2014.

[14] M. I. DYAKONOV. Spin hall effect. *International journal of modern physics. B, Condensed matter physics, statistical physics, applied physics*, 23:2556–EOA, 08 2009.

[15] Luqiao Liu, Chi-Feng Pai, Y. Li, H. W. Tseng, D. C. Ralph, and R. A. Buhrman. Spin-torque switching with the giant spin hall effect of tantalum. *Science*, 336(6081):555–558, 2012.

[16] Chunhui Du, Hailong Wang, Fengyuan Yang, and P. Chris Hammel. Systematic variation of spin-orbit coupling with d-orbital filling: Large inverse spin hall effect in $3d$ transition metals. *Phys. Rev. B*, 90:140407, Oct 2014.

[17] Ting Wang, Wei Wang, Yunsong Xie, Mohammed A. Warsi, Jun Wu, Yuanzhen Chen, Virginia O. Lorenz, Xin Li Fan, and John Q. Xiao. Large spin hall angle in vanadium film. In *Scientific Reports*, 2017.

[18] Takuro Tanaka and Hiroshi Kontani. Extrinsic Spin Hall Effect Due to Transition-Metal Impurities. *Progress of Theoretical Physics*, 128(5):805–828, 11 2012.

[19] Neal Reynolds, Priyamvada Jadaun, John T. Heron, Colin L. Jermain, Jonathan Gibbons, Robyn Collette, R. A. Buhrman, D. G. Schlom, and D. C. Ralph. Spin Hall torques generated by rare-earth thin films. *Physical Review B*, 95:064412, February 2017.

[20] Jack Bass and William P Pratt. Spin-diffusion lengths in metals and alloys, and spin-flipping at metal/metal interfaces: an experimentalist's critical review. *Journal of Physics: Condensed Matter*, 19(18):183201, apr 2007.

[21] T. Kimura, J. Hamrle, and Y. Otani. Estimation of spin-diffusion length from the magnitude of spin-current absorption: Multiterminal ferromagnetic/nonferromagnetic hybrid structures. *Phys. Rev. B*, 72:014461, Jul 2005.

[22] Martin Gradhand, Dmitry V. Fedorov, Peter Zahn, and Ingrid Mertig. Spin hall angle versus spin diffusion length: Tailored by impurities. *Phys. Rev. B*, 81:245109, Jun 2010.

[23] Qiang Hao, Wenzhe Chen, and Gang Xiao. Beta (Î) tungsten thin films: Structure, electron transport, and giant spin hall effect. *Applied Physics Letters*, 106:182403, 05 2015.

[24] Jack T. Brangham, Keng-Yuan Meng, Angela S. Yang, James Gallagher, Bryan Esser, Shane P. White, Sisheng Yu, David W. McComb, P Chris Hammel, and Fengyuan Yang. Thickness dependence of spin hall angle of au grown on y3fe5o12 epitaxial films. *Physical Review B*, 94, 08 2016.

[25] Qiang Hao and Gang Xiao. Giant spin hall effect and switching induced by spin-transfer torque in a $W/co_{40}fe_{40}b_{20}/MgO$ structure with perpendicular magnetic anisotropy. *Phys. Rev. Applied*, 3:034009, Mar 2015.

[26] Y. S. Kang, C. Y. Kim, M. H. Cho, K. B. Chung, C. H. An, H. Kim, H. J. Lee, C. S. Kim, and T. G. Lee. Thickness dependence on crystalline structure and interfacial reactions in hfo2 films on inp (001) grown by atomic layer deposition. *Applied Physics Letters*, 97(17):172108, 2010.

[27] P. Laczkowski, Y. Fu, H. Yang, J.-C. Rojas-Sánchez, P. Noel, V. T. Pham, G. Zahnd, C. Deranlot, S. Collin, C. Bouard, P. Warin, V. Maurel, M. Chshiev, A. Marty, J.-P. Attané, A. Fert, H. Jaffrès, L. Vila, and J.-M. George. Large enhancement of the spin hall effect in au by side-jump scattering on ta impurities. *Phys. Rev. B*, 96:140405, Oct 2017.

[28] Wenzhe Chen, Gang Xiao, Qiang Zhang, and Xixiang Zhang. Temperature study of the giant spin hall effect in the bulk limit of -w. *Physical review. B, Condensed matter*, 98:134411, 10 2018.

[29] Miren Isasa, Estitxu Villamor, Luis E. Hueso, Martin Gradhand, and Fèlix Casanova. Temperature dependence of spin diffusion length and spin hall angle in au and pt. *Phys. Rev. B*, 91:024402, Jan 2015.

[30] Y. Niimi, Y. Kawanishi, D. H. Wei, C. Deranlot, H. X. Yang, M. Chshiev, T. Valet, A. Fert, and Y. Otani. Giant Spin Hall Effect Induced by Skew Scattering from Bismuth Impurities inside Thin Film CuBi Alloys. , 109:156602, October 2012.

[31] Zhenyao Tang, Yuta Kitamura, Eiji Shikoh, Yuichiro Ando, Teruya Shinjo, and Masashi Shiraishi. Temperature dependence of spin hall angle of palladium. *Applied Physics Express*, 6(8):083001, aug 2013.

[32] Martin Gradhand, Dmitry V. Fedorov, Peter Zahn, and Ingrid Mertig. Extrinsic spin hall effect from first principles. *Phys. Rev. Lett.*, 104:186403, May 2010.

[33] H. L. Wang, C. H. Du, Y. Pu, R. Adur, P. C. Hammel, and F. Y. Yang. Scaling of Spin Hall Angle in 3d, 4d, and 5d Metals from $Y_3Fe_5O_{12}$/Metal Spin Pumping. , 112:197201, May 2014.

[34] O. Mosendz, J. E. Pearson, F. Y. Fradin, G. E. W. Bauer, S. D. Bader, and A. Hoffmann. Quantifying spin hall angles from spin pumping: Experiments and theory. *Phys. Rev. Lett.*, 104:046601, Jan 2010.

[35] P. Laczkowski, J. C. Rojas-Sánchez, W. Savero-Torres, H. Jaffrès, N. Reyren, C. Deranlot, L. Notin, C. Beigné, A. Marty, J. P. Attané, L. Vila, J. M. George,

and A. Fert. Experimental evidences of a large extrinsic spin Hall effect in AuW alloy. *Applied Physics Letters*, 104:142403, Apr 2014.

[36] J. Wu, L. Zou, T. Wang, Y. Chen, J. Cai, J. Hu, and J. Q. Xiao. Spin hall angle and spin diffusion length in au–cu alloy. *IEEE Transactions on Magnetics*, 52(7):1–4, July 2016.

[37] B. Gu, I. Sugai, T. Ziman, G. Y. Guo, N. Nagaosa, T. Seki, K. Takanashi, and S. Maekawa. Surface-Assisted Spin Hall Effect in Au Films with Pt Impurities. , 105:216401, November 2010.

[38] Y. Niimi, M. Morota, D. H. Wei, C. Deranlot, M. Basletic, A. Hamzic, A. Fert, and Y. Otani. Extrinsic spin hall effect induced by iridium impurities in copper. *Phys. Rev. Lett.*, 106:126601, Mar 2011.

[39] Wei Zhang, Matthias B. Jungfleisch, Wanjun Jiang, John E. Pearson, Axel Hoffmann, Frank Freimuth, and Yuriy Mokrousov. Spin hall effects in metallic antiferromagnets. *Phys. Rev. Lett.*, 113:196602, Nov 2014.

[40] Jun Liu, Tadakatsu Ohkubo, Seiji Mitani, Kazuhiro Hono, and Masamitsu Hayashi. Correlation between the spin hall angle and the structural phases of early 5d transition metals. *Applied Physics Letters*, 107(23):232408, 2015.

[41] Z. Qiu, T. An, K. Uchida, D. Hou, Y. Shiomi, Y. Fujikawa, and E. Saitoh. Experimental investigation of spin hall effect in indium tin oxide thin film. *Applied Physics Letters*, 103(18):182404, 2013.

[42] M. Morota, Y. Niimi, K. Ohnishi, D. H. Wei, T. Tanaka, H. Kontani, T. Kimura, and Y. Otani. Indication of intrinsic spin Hall effect in 4d and 5d transition metals. *Physical Review B*, 83:174405, May 2011.

[43] Andrew J. Berger, Eric R. J. Edwards, Hans T. Nembach, Olof Karis, Mathias Weiler, and T. J. Silva. Determination of the spin hall effect and the spin diffusion length of pt from self-consistent fitting of damping enhancement and inverse spin-orbit torque measurements. *Phys. Rev. B*, 98:024402, Jul 2018.

[44] Rui Wang, Zhengyu Xiao, Huihui Liu, Zhiyong Quan, Xiao Zhang, Meimei Wang, Mingzhong Wu, and Xiaohong Xu. Enhancement of perpendicular magnetic anisotropy and spin-orbit torque in ta/pt/co/ta multi-layered heterostructures through interfacial diffusion. *Applied Physics Letters*, 114(4):042404, 2019.

[45] Simranjeet Singh, Marta Anguera, Enrique del Barco, Ross Springell, and Casey W. Miller. Moderate positive spin hall angle in uranium. *Applied Physics Letters*, 107(23):232403, 2015.

Appendix A:
Raw Data

The data used in the graphs in Section 3 is listed in the following table along with the sources. The table is organized alphabetically by the material being studied.

Material	temp(K)	spin diffusion length(nm)	length uncertainty	resistivity ($\mu\Omega$*cm)	spin hall angle(%)	angle uncertainty	thickness(nm)	notes	source
Ag	295	700	15	142.8571429	0.1				[3]
Ag				6.6	0.68	0.07			[33]
Al	4.2	455	15	9.523809524	0.032	0.006			[3]
Al	4.2	705	30	5.882352941	0.016	0.004			[3]
Au	295	86	10	2.702702703	11.3				[3]
Au	295	83		2.702702703	3				[3]
Au	4.5	65		2.070393375	< 2.3				[3]
Au	295	36		3.891050584	<2.7				[3]
Au	295	35	4	3.571428571	7	0.1			[3]
Au	295	27	3	7.142857143	7	0.3			[3]
Au	295	25	3	6.896551724	12	4			[3]
Au	295	50	8	5.988023952	0.8	0.2			[3]
Au	<10	40	16	4	1.4	0.4			[3]
Au	295	35	3	3.968253968	0.35	0.03			[3]
Au	295	35		5	0.25	0.1			[3]
Au	295	35	3	19.04761905	1.6	0.1			[3]
Au	295	35	3	14.28571429	0.335	0.006			[3]
Au	295	35			1.1	0.3			[3]
Au	295	60		4.901960784	8.4	0.7			[3]
Au		35	3	44.44444444	0.16	0.03			[34]
Au	10				1.4	0.4	20		[35]
Au		12.6			8.7		5		[24]
Au		12.6			3.8		10		[24]
Au		12.6			1.8		20		[24]
Au		12.6			2		30		[24]
Au		12.6			1.6		50		[24]
Au		12.6			1.7		100		[24]
Au(1-x)Ta(x)		4.75	0.75		19		5	x=0.025,estimated from graph	[27]
Au(1-x)Ta(x)		2.3	0.1		33		5	x=0.05,estimated from graph	[27]
Au(1-x)Ta(x)		1.95	0.75		39		5	x=0.075,estimated from graph	[27]
Au(1-x)Ta(x)		1.8	0.1		36		5	x=0.1,estimated from graph	[27]
Au(1-x)Ta(x)		2.3	0.1		38.5		10	x=0.05,estimated from graph	[27]
Au(1-x)Ta(x)		1.8	0.1		53		10	x=0.1,estimated from graph	[27]
Au(1-x)Ta(x)		4.75	0.75		15		15	x=0.025,estimated from graph	[27]
Au(1-x)Ta(x)		2.3	0.1		29		15	x=0.05,estimated from graph	[27]
Au(1-x)Ta(x)		1.95	0.75		34		15	x=0.075,estimated from graph	[27]
Au(1-x)Ta(x)		1.8	0.1		25.5		15	x=0.1,estimated from graph	[27]
Au(1-x)W(x)		13			0			x=0.01,estimated from graph	[27]
Au(1-x)W(x)		5.5			3			x=0.03,estimated from graph	[27]
Au(1-x)W(x)		3			5			x=0.05,estimated from graph	[27]
Au(1-x)W(x)		2			8			x=0.07,estimated from graph	[27]
Au(1-x)W(x)					11.5			x=0.1,estimated from graph	[27]
Au(1-x)W(x)		1.5			14			x=0.14,estimated from graph	[27]
Au(1-x)W(x)		1.2			6			x=0.16,estimated from graph	[27]
Au(1-x)W(x)					4			x=0.17,estimated from graph	[27]
Au(1-x)W(x)					-6			x=0.28,estimated from graph	[27]
Au(60)Cu(40)		5		11.63	1.3	2			[36]
Au(98.6)Pt(1.4)	300	25	3	6.9	12	4	10		[37]
Au(98.6)Pt(1.4)	300	50	8	6	0.8	0.2	20		[37]
Au(C impurities)					9	0.1		estimated from graph	[32]
Au(Li impurities)					0.8	0.1		estimated from graph	[32]
Au(Mg impurities)					-0.8	0.1		estimated from graph	[32]

Material	temp(K)	spin diffusion length(nm)	length uncertainty	resistivity ($\mu\Omega$*cm)	spin hall angle(%)	angle uncertainty	thickness(nm)	notes	source
Au(N impurities)					6.3	0.1		estimated from graph	[32]
Au(Pt impurities)					1	0.1		estimated from graph	[32]
Au(x)Pt(1-x)	300	1.2	0.1		14.5	0.5		x=0, estimated from graph	[8]
Au(x)Pt(1-x)	300	1.05	0.1		13	3		x=.2+-.05, estimated from graph	[8]
Au(x)Pt(1-x)	300	0.95	0.1		18	2		x=.275+=.05, estimated from graph	[8]
Au(x)Pt(1-x)	300	0.8	0.1		17	3		x=.325+-.05, estimated from graph	[8]
Au(x)Pt(1-x)	300	0.7	0.1		17.5	3		x=.48+-.05, estimated from graph	[8]
Au(x)Pt(1-x)	300	0.3	0.1		32	5		x=.52+-.05, estimated from graph	[8]
Au(x)Pt(1-x)	300	0.9	0.1		10	0.5		x=.7+-.05, estimated from graph	[8]
Au(x)Pt(1-x)	300	2.88	0.1		6	0.5		x=.71+-.05, estimated from graph	[8]
Au(x)Pt(1-x)	300	34	0.5		5	0.5		x=1, estimated from graph	[8]
Au(Zn impurities)					-1.8	0.1		estimated from graph	[32]
Au(Zn impurities)					0.5	0.1		estimated from graph	[32]
AuW	295	1.9		57.14285714	>10				[3]
AuW		1.9		57	10		20		[35]
Bi	3	0.3	0.1		>0.3				[3]
Bi	295				.7.1	0.8			[3]
Bi					1.9	0.2.V.			[3]
Cr		13.3		112	-5.1	0.5			[16]
Cu	295	500		830	0.32	0.03			[3]
Cu		500		6.25	0.32	0.03			[16]
Cu				630	0.32	0.03			[33]
Cu(99.5)Bi(.5)	10	100; 30		0	-11	4			[3, 6, 30]
Cu(C impurities)					0.7	0.05		estimated from graph	[32]
Cu(Li impurities)					0.24	0.05		estimated from graph	[32]
Cu(Mg impurities)					-0.15	0.05		estimated from graph	[32]
Cu(N impurities)					0.75	0.05		estimated from graph	[32]
Cu(Pt impurities)					2.65	0.05		estimated from graph	[32]
Cu(Zn impurities)					-0.2	0.05		estimated from graph	[32]
Cu(Zn impurities)					0.05	0.05		estimated from graph	[32]
CuIr	10	5–30			2.1	0.6			[3, 6, 38]
Fe					0.9				[]
Fe(20)Ni(80)		1.7			2	0.5			[16]
Fe(50)Mn(50)		2.8			-0.0074	800			[16]
FeMn		1.8	0.5	280	0.8	0.2			[39]
Hf				167.7	11				[40]
Hf(amorphous)		0.3			11				[40]
Hf(hexagonal close packed)		1.3		1	7				[40]
Indium tin oxide(ITO)		30	2	155	0.65	0.1			[41]
InSb	1.3				0.026	0.005			[3]
InSb	1.3								[3]
IrMn		0.7	0.2		2.2	0.5			[39]
IrMn				269.3	-4.4	0.4			[]
IrO2	300	3.8(P)			4,6.5(P);				[3]
Mn		10.7	1.1	555.5555556	-0.19	0.01			[16]
Mo	10	10		980	-0.2				[3]

Material	temp(K)	spin diffusion length(nm)	length uncertainty	resistivity ($\mu\Omega$*cm)	spin hall angle(%)	angle uncertainty	thickness(nm)	notes	source
Mo	10	10		33.00330033	-0.075				[3]
Mo	10	8.6	1.3	149.9250375	-0.8	0.18			[3]
Mo	295	35	3	35.71428571	-0.05	0.01			[3]
Mo		35	3	21.45922747	-0.023	0.005			[34]
Mo		8.6	1.3	21.45922747	-0.8	0.18	20		[42]
n-GaAs	4.2	2200		116	0.15				[3]
n-GaAs	4.2	8500		17857.14286	0.08				[3]
n-GaAs	30	0.0036		72992.70073					[3]
n-GaAs	2			1250	-0.001				[3]
n-GaAs	295				0.00044;	0.001			[3]
n-InGaAs	30	3000			0.02				[3]
Nb	10	5.9	0.3	50000	-0.87	0.2			[3]
Nb		5.9	0.3	90.90909091	-0.87	0.2	11		[42]
Ni		3.2	0.1	57	4.9	0.5			[16]
p-Si	295				0.01				[3]
Pd	10	13	2		1.2	0.4			[3]
Pd	295	9		45.45454545	1				[3]
Pd	295	15	4	50.76142132	0.64	0.1			[3]
Pd	295	5.5	0.5	25	1.2	0.3			[3]
Pd	295	2	0.1	20	0.8	0.2			[3]
Pd		13	2	27.02702703	1.2	0.4	20		[42]
Pd	130			112	2.25			estimated from graph	[31]
Pd	170				1.75			estimated from graph	[31]
Pd	210				1.45			estimated from graph	[31]
Pd	255				1.3			estimated from graph	[31]
Pd	295				1.1			estimated from graph	[31]
Pd(6)Py(t)	300				4.3		2	estimated from graph	[9]
Pd(6)Py(t)	300				5.2		3	estimated from graph	[9]
Pd(6)Py(t)	300				6		4	estimated from graph	[9]
Pd(6)Py(t)	300				6.5		5	estimated from graph	[9]
Pd(6)Py(t)	300				7.5		6	estimated from graph	[9]
Pd(6)Py(t)	300				7.4		7	estimated from graph	[9]
Pd(6)Py(t)	300				7		8	estimated from graph	[9]
Pd(6)Py(t)	300				7.4		10	estimated from graph	[9]
Pd(t)Py(4)	300				4.2		2	estimated from graph	[9]
Pd(t)Py(4)	300				5		3	estimated from graph	[9]
Pd(t)Py(4)	300				5.2		4	estimated from graph	[9]
Pd(t)Py(4)	300				5.5		5	estimated from graph	[9]
Pd(t)Py(4)	300				5.6		6	estimated from graph	[9]
Pd(t)Py(4)	300				5.8		7	estimated from graph	[9]
Pd(t)Py(4)	300				5.9		8	estimated from graph	[9]
Pd(t)Py(4)	300				5.8		10	estimated from graph	[9]
Pd(t)Py(4)	300				5.8		12	estimated from graph	[9]
Pd(t)Py(4)	300				5.8		14	estimated from graph	[9]
PdMn		1.3	1		1.5	0.5			[39]
Pt	295			233	0.37				[3]
Pt	5	8			0.44				[3]
Pt	295	7		12.5	5.56	0.9			[3]
Pt	10	11	2		2.1	0.5			[3]
Pt	10	10		12.34567901	2.4				[3]
Pt	295	7		12.34567901	6.4	8			[3]
Pt	295	10	2		1.3	0.2			[3]

Material	temp(K)	spin diffusion length(nm)	length uncertainty	resistivity ($\mu\Omega$*cm)	spin hall angle(%)	angle uncertainty	thickness(nm)	notes	source
Pt	295	10		41.66666667	2	4			[3]
Pt	295	3.7	0.2		8	1			[3]
Pt	295	8.3	0.9	41.32231405	1.2	0.2			[3]
Pt	295	7.7	0.7	23.25581395	1.3	0.1			[3]
Pt	295	1.5-10		76.92307692	3				[3]
Pt	295	4		40.81632653	2.7	0.5			[3]
Pt	295	8	1	25	2.012	0.003			[3]
Pt	295	1.3		98.03921569	2.1	1.5			[3]
Pt	295	1.2		41.66666667	8.6	0.5			[3]
Pt	295	1.4			12	4			[3]
Pt	295	3.4	0.4		5.6	0.1			[3]
Pt	295	7.3		16.66666667	10	1			[3]
Pt	295	1.2	0.1	47.61904762	2.2	0.4			[3]
Pt	295	3.<6.		27.77777778	7.6				[3]
Pt	295	2.1	0.2	20	2.2	0.8			[3]
Pt	295	2.1	0.2	27.77777778	8.5	0.9			[3]
Pt	295	2.4		27.77777778	4				[3]
Pt	295	1.5	0.5	83.33333333	11	8			[3]
Pt	300	1.5		100	6.8	0.25	6		[9]
Pt					38.7	0.8			[43]
Pt		10	2		0.67	0.06			[34]
Pt		11	1	41.32231405	2.1	5	20		[42]
Pt	13				5.5			estimated from graph	[9]
Pt	25				5.7			estimated from graph	[9]
Pt	50				5.8			estimated from graph	[9]
Pt	150				5.75			estimated from graph	[9]
Pt	175				6			estimated from graph	[9]
Pt	200				6.2			estimated from graph	[9]
Pt	225				6			estimated from graph	[9]
Pt	250				6.4			estimated from graph	[9]
Pt	275				6.2			estimated from graph	[9]
Pt	300				6.8			estimated from graph	[9]
Pt/Fe/Al					6.2				[]
PtMn		0.5	0.1		6	0.1			[39]
Re(amorphous and hexagonal close packed)		1.5		164	4				[40]
Re(hexagonal closed pack				102					[40]
Ru				0	0.3				[?]
Si	30				0.1-0.38				[3]
Ta	10	2.7	0.4		-0.37	0.11			[3]
Ta	295	1.9		333.3333333	-7.1	0.6			[3]
Ta	295	1.8	0.7	294.1176471	-2				[3]
Ta	295			133.3333333	-12	3			[3]
Ta	295	1.5	0.5		-3	1			[3]
Ta	300			200	11.18	1.118			[1]
Ta	250				11.07	1.107			[1]
Ta	200				11.22	1.122			[1]
Ta	150				12.4	1.24			[1]
Ta	100				12.99	1.299			[1]
Ta	50				12.39	1.249			[1]
Ta	5				14.2	1.42			[1]
Ta	295						2	xrd, estimated from graph	[5]
Ta	295						4	xrd, estimated from graph	[5]
Ta	295						7	xrd, estimated from graph	[5]
Ta	295						8	xrd, estimated from graph	[5]
Ta	295						9	xrd, estimated from graph	[5]
Ta	295						10	xrd, estimated from graph	[5]

Material	temp(K)	spin diffusion length(nm)	length uncertainty	resistivity ($\mu\Omega$*cm)	spin hall angle(%)	angle uncertainty	thickness(nm)	notes	source
Ta	295						15	xrd, estimated from graph	[5]
Ta	295						16	xrd, estimated from graph	[5]
Ta	295						20	xrd, estimated from graph	[5]
Ta	295						30	xrd, estimated from graph	[5]
Ta	295						40	xrd, estimated from graph	[5]
Ta	295						50	xrd, estimated from graph	[5]
Ta	295	5.1	0.6		-0.62	0.1		xrd, estimated from graph	[5]
Ta		2.7	0.4		-0.37	0.11	20		[42]
Ta-W				11.63	27				[]
Ta(0.5)—Re(amorphous)		1		172	7				[40]
Ta(amorphous)		0.4			10				[40]
Ta/Pt/Co/Ta				159	61	3			[44]
Ti		13.3			-0.036	0.004			[16]
U				300	0.4				[45]
V	RT	16.3	7		-0.1	0.1	2	estimated from graph	[17]
V	RT	16.3	7	280	-2.3	0.1	5	estimated from graph	[17]
V	RT	16.3	7	260	-5	0.2	10	estimated from graph	[17]
V	RT	16.3	7	250	-7.1	0.3	30	estimated from graph	[17]
V	RT	16.3	7	235	-6.5	0.5	50	estimated from graph	[17]
V		14.9	2.4	225	-1	0.1			[16]
W	295	2.1		290	-14	1			[3]
W	295			181.8181818	-33	6			[3]
W	300	3.5	0.3		40	3		estimated from graph	[25]
W	300	3.5	0.3		14	1	3	estimated from graph	[25]
W	300	3.5	0.3		18	2	4.5	estimated from graph	[25]
W	300	3.5	0.3		26.5	3	5	estimated from graph	[25]
W	300	3.5	0.3		22.5	3	5.5	estimated from graph	[25]
W	300	3.5	0.3		26	3	6	estimated from graph	[25]
W	300	3.5	0.3		27	3	6.5	estimated from graph	[25]
W	300	3.5	0.3		30	3.5	7	estimated from graph	[25]
W	300	3.5	0.3		33	3.5	8	estimated from graph	[25]
W	300	3.5	0.3		35	4	9	estimated from graph	[25]
W	10				49.578	2.108	15		[28]
W	100				50.238	1.144	15		[28]
W	200				52.534	1.4	15		[28]
W	300				50.052	1.5	15		[28]
W	300				57	2	18		[28]
W	300	3.9	0.3		56	3	infinity		[28]
W	300				43	2	12		[28]
W	300				65	2	18	taking into account spin transmission probability	[28]
W	300				64	3	infinity	taking into account spin transmission probability	[28]
W(body centered cubic)									[40]
W(amorphous and body centered cubic)		1.3		0	23				[40]